Environmental Pollution 372 (2025) 125995

Contents lists available at ScienceDirect

Environmental Pollution

journal homepage: www.elsevier.com/locate/envpol

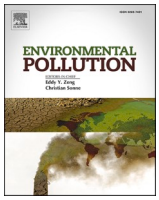

PM_{10}-bound elements in Luanda's urban atmosphere: Concentrations, sources, and their environmental and health impacts☆

Célia A. Alves [a,*], Ana Sanchez de la Campa [b,c], Yago Cipoli [a], Leonardo Furst [a], Gustavo Higawa [a], Anabela Leitão [d], Alan Victor da Silva [a], Manuel S. Feliciano [e]

[a] Department of Environment and Planning, Centre for Environmental and Marine Studies (CESAM), University of Aveiro, Aveiro, 3810-193, Portugal
[b] Associate Unit CSIC-University of Huelva "Atmospheric Pollution", Centre for Research in Sustainable Chemistry - CIQSO, University of Huelva, E21071, Huelva, Spain
[c] Department of Earth Sciences, Faculty of Experimental Sciences, University of Huelva, Huelva, 21007, Spain
[d] LESRA – Laboratório de Engenharia da Separação, Reação e Ambiente, Universidade Agostinho Neto, Av. Ho Chi Minh nº 201, Luanda, Angola
[e] CIMO, LA SusTEC, Instituto Politécnico de Bragança, Campus de Santa Apolónia, 5300- 253, Bragança, Portugal

ARTICLE INFO

Keywords:
Luanda
PM_{10}
Elements
Contamination indices
Health risks

ABSTRACT

An unprecedented study was carried out in the megacity of Luanda, Angola, involving daily sampling of particulate matter (PM_{10}) from June to November 2023. The analysis was focused on the detection of 56 metal(loid)s and complemented by the application of several contamination and health risk indices. PM_{10} levels ranged from 23.6 to 108 μg/m^3, averaging 59.3 μg/m^3, exceeding WHO's 24-h guideline on 83% of days. In addition to crustal elements, the most abundant constituents were Zn (159 ng/m^3), Ba (43.2 ng/m^3), Pb (17.8 ng/m^3), Cu (10.5 ng/m^3), Sr (7.0 ng/m^3), Ni (4.5 ng/m^3), Sb (3.7 ng/m^3) and Cr (3.5 ng/m^3). Mineral dust, primarily from unpaved roads and local soils, accounted for 31 wt% of PM_{10}, while sea salt contributed 6%. Geochemical markers (e.g., Ce-La-V relationships) suggest that vanadium originates predominantly from upper crust weathering. Elemental ratios such as Fe/Cu, Cu/Sb, and Zn/Sb indicate significant contributions from traffic-related emissions (e.g., brake and tyre wear) and industrial sources. Sulphur, an important PM_{10} component, likely stems from fossil fuel combustion and petroleum refining. Luanda experiences severe air pollution, with high inputs from Sb, Cd, Zn, and other elements linked to traffic, industrial emissions, and biomass burning. The extremely high ecological risk (RI = 4360 ± 2440) highlights critical contamination, driven primarily by Cd and Sb, while the Nemerow risk index (1990 ± 1530) underscores urgent public health concerns. Non-cancer hazard indices (HI) exceeded safe thresholds for children (2.29) and adults (2.18), with Fe, Mn, Be, Pb, Ni, Co, and Sb identified as key contributors. Carcinogenic risks from PM_{10} inhalation (2.34×10^{-3} for children and 1.36×10^{-3} for adults) also exceeded acceptable levels, emphasising the need for targeted pollution mitigation strategies.

1. Introduction

The latest State of Global Air report (HEI, 2024) highlights that, in 2021, air pollution was the second leading risk factor for premature death globally, surpassed only by high blood pressure. It was responsible for approximately 1 in 8 deaths, accounting for 8.1 million deceases worldwide, with particular incidence in South Asian and African countries. More than 90% of the total air pollution disease burden was attributed to particulate matter. In fact, it is well known that particulate matter with a diameter lower than 10 or 2.5 μm (PM_{10} and $PM_{2.5}$, respectively) poses serious health risks. Due to their small size, these particles can penetrate deeply into the lungs, leading to a variety of respiratory and cardiovascular diseases (Guo et al., 2023; Kyung and Jeong, 2020). Vulnerable populations, including children, the elderly, people with preexisting conditions and low-income communities, are disproportionately affected by the detrimental effects of particulate matter (Sacks et al., 2011).

Several studies across various cell lines have shown that coarse particulate matter ($PM_{2.5\text{-}10}$) can exhibit cytotoxic, genotoxic, and inflammatory effects that are equal to or even exceed those of fine PM (e.

☆ This paper has been recommended for acceptance by Eddy Y. Zeng.

* Corresponding author.
E-mail address: celia.alves@ua.pt (C.A. Alves).

https://doi.org/10.1016/j.envpol.2025.125995
Received 2 January 2025; Received in revised form 2 March 2025; Accepted 3 March 2025
Available online 4 March 2025

g., Kataoka et al., 2021; Schins et al., 2022; Jarvis et al., 2018; Tang et al., 2020; Spagnolo et al., 2015; Sarkar et al., 2019). A systematic review and meta-analysis by Adar et al. (2014) found that increased levels of $PM_{2.5-10}$ were associated with higher morbidity and mortality from respiratory and cardiovascular causes, while similar correlations for $PM_{2.5}$ were not consistently robust. Additionally, Brunekreef and Forsberg (2005) concluded that coarse PM has short-term effects on asthma, chronic obstructive pulmonary disease, and respiratory admissions that are as strong as or stronger than those of fine PM. Given that PM_{10} encompasses smaller size fractions, it serves as a reliable proxy for overall toxicity and an integrative indicator of potential health impacts.

PM_{10} originates from a wide range of sources, both primary and secondary, including vehicular emissions, industrial activities, biomass burning, resuspended road dust, and natural sources such as sea spray and mineral dust transport. In urban environments, traffic emissions, brake and tyre wear, and construction activities significantly contribute to PM_{10} levels (Amato et al., 2016; Hopke et al., 2020). Studies have shown that PM_{10}-bound metal(loid)s play a key role in toxicity, particularly transition metals such as Cu, Mn, and Fe, which can catalyse the formation of reactive oxygen species (ROS) upon inhalation. This oxidative stress is a major pathway for tissue damage and inflammation, potentially leading to respiratory and cardiovascular diseases (Lin and Yu, 2019; Lin and Yu, 2020; Rodrigo-Moreno et al., 2013; Santibáñez-Andrade et al., 2023). Some metal(loid)s, such as As, Cd, Cr, Pb and Hg, are very hazardous to living organisms even at low concentrations, and rank among the priority pollutants. Epidemiological and experimental studies have led the United States Environmental Protection Agency (USEPA) and the International Agency for Research on Cancer (IARC) to classify these elements as either "known" or "probable" human carcinogens (Tchounwou et al., 2012).

Despite Africa being one of the most impacted continents by particulate air pollution, reliable, long-term air quality monitoring remains largely absent. Only a few countries, such as Senegal, South Africa, Rwanda, and Morocco, have established reference-grade monitoring networks (HEI, 2024), while the characterisation of PM_{10} and/or $PM_{2.5}$ metal(loid)s across African cities remains sparse (Boman et al., 2013; Edlund et al., 2021; Gaita et al., 2014; Kolawole and Olatunji, 2023; Kumar et al., 2024; Shetaya et al., 2024; Sulaymon et al., 2020; Tefera et al., 2020). In Angola, there is no established air quality monitoring network, and studies on the elemental composition of PM are virtually non-existent. This critical knowledge gap limits the identification of pollution sources, hinders risk assessments, and prevents the implementation of targeted mitigation strategies.

To address this urgent need, we conducted the first long-term PM_{10} measurement campaign in Luanda, a rapidly growing megacity with intense vehicular traffic, industrial activities, and extensive unpaved road networks. This study provides a comprehensive chemical characterisation of PM_{10}-bound metal(loid)s, identifies key emission sources, and quantifies the associated environmental and health risks. Given that resuspended dust and traffic-related emissions are major contributors to airborne pollution in Luanda, PM_{10} serves as a more representative indicator of exposure risks compared to $PM_{2.5}$, as it encompasses both fine and coarse fractions influenced by local pollution sources. The findings offer crucial insights into atmospheric pollution levels and serve as a scientific basis for future air quality management policies in Angola and other under-monitored regions.

2. Methodology

2.1. Sampling

Luanda, the capital of Angola, is located on the Atlantic coast in the north of the country. It is the country's largest city and one of its busiest seaports. It constitutes a municipality subdivided into six urban districts and is also the capital of the province of the same name. Luanda has a tropical savanna climate characterised by warm temperatures year-round, a distinct wet season from October to April, and a dry season from May to September. In 2020, the metropolitan area had a population exceeding 8.3 million residents. Greater Luanda is primarily engaged in oil production, construction, fisheries, and manufacturing, with a growing emphasis on services and trade. Sampling was carried out in the centre of Luanda, on the roof of the guardhouse at the entrance to the Faculty of Engineering of the Agostinho Neto University (8°50′49″S; 13°13′51″E), at an approximate height of 3 m. The facilities are located on an avenue with heavy traffic that gives access to the old airport of the Angolan capital. PM_{10} samples were collected every day over 24-h periods, beginning at 6:00 a.m. local time, from June 25 to November 6, 2023, using a high-volume sampler from AMS Analitica® (Italy). This sampler complies with the EN 12341:2023 (Ambient air - Standard gravimetric measurement method for the determination of the PM_{10} or $PM_{2.5}$ mass concentration of suspended particulate matter) and operates at a flow rate of 500 L/min. It was equipped with 150 mm quartz fibre filters from Pall. A total of 129 PM_{10} samples were collected.

2.2. Analytical determinations

PM_{10} filters were weighted using an analytical microbalance (Radwag 5/2Y/F) with 1 μg readability. Gravimetric concentrations were determined by averaging six weighings following a stabilisation period of 48–72 h in a temperature- and humidity-controlled environment (20 °C and 50% humidity).

Major and trace elements were quantified following acid digestion of PM_{10} filters. Two filter sections (7 cm^2 each) were digested in a strong acid mixture (1.25 mL HNO_3, 2.5 mL HF, and 1.25 mL $HClO_4$) within 60 mL Savillex vessels on a hot plate, following the procedure described by Querol et al. (2001).

Analysis was conducted with an inductively coupled plasma optical emission spectrometer (ICP-OES, AGILENT 5110) and an inductively coupled plasma mass spectrometer (ICP-MS, AGILENT 7900), following a protocol adapted from Querol et al. (2001). Each analytical run included the assessment of a fly ash standard reference material (NIST-1633c) for quality control. To do this, blank filters were impregnated with the reference material and analysed alongside the samples, employing ^{103}Rh as an internal standard to minimise potential plasma fluctuations. Multi-elemental solutions from Agilent® were used for external calibration. For ICP-MS, external calibration was performed using cocktail solutions (1, 10, 50, 100 and 250 ppb as well as a HNO_3 5% blank). For ICP-OES, external calibration was carried out using elemental standard solutions in the range from 0.05 to 100 ppm, along with a 5% HNO_3 blank. For all elements, the calibration curves exhibited correlation coefficients above 0.999, ensuring high accuracy in element quantification. The average precision and accuracy for most elements were in the range from 5 to 10%. To achieve this, an analysis of the standard reference material (NIST-1633c) was performed using both techniques. For every 10 samples, a field blank filter was kept, whose concentrations were subtracted from those of PM_{10}. A comprehensive study with 47 laboratory filters was recently conducted to assess element concentrations, applying the same digestion and analytical procedures. The results can be found in the supplementary material (Table S1).

2.3. Backward air mass trajectory analysis

Backward air mass trajectories arriving at Luanda were calculated every 24 h with a run time of 120 h and an arrival height of 500 m above the ground level using the HYSPLIT (HYbrid Single-Particle Lagrangian Integrated Trajectory) model provided by the U.S. National Oceanic and Atmospheric Administration (NOAA) (Stein et al., 2015; Rolph et al., 2017). The model was run with the National Centres for Environmental Prediction/National Center for Atmospheric Research (NCEP/NCAR) reanalysis dataset (2.5° spatial resolution). The trajectories were assigned to 4 clusters using an automated K-means clustering algorithm

Table 1
Indices calculated in this study to assess contamination degrees and risks associated with ambient PM_{10} in Luanda.

Indices	Equations	Eq. number	Explanations	Contamination or risk degree
Crustal enrichment factor (Alves et al., 2020)	$CEF_i = (C_i/Al)_{air}/(C_i/Al)_{crust}$	(7)	$(C_i/Al)_{air}$ is the concentration ratio of element i to Al in the PM_{10} samples, and $(C_i/Al)_{crust}$ is the concentration ratio of element i to Al in the upper continental crust (Wedepohl, 1995)	<2 minimal enrichment [2,5[moderate enrichment [5,20[significant enrichment [20,40[very high enrichment ≥40 extremely high enrichment
Marine enrichment factor (Conca et al., 2019)	$MEF_i = (C_i/Na)_{air}/(C_i/Na)_{sea}$	(8)	$(C_i/Na)_{air}$ is the concentration ratio of element i to Na in the PM_{10} samples, and $(C_i/Na)_{sea}$ is the concentration ratio of element i to Na in sea water	<10 no enrichment [10,100[minor enrichment ≥100 non-marine origin
Geoaccumulation index (Alves et al., 2020)	$I_{geoi} = \log_2 \frac{C_i}{1.5B_i}$	(9)	C_i is the concentration of element I; B_i is the geochemical background value of each element; due to the lack of data for Angolan soils or dust, the Earth's upper crust values from Wedepohl (1995) were adopted.	<0 uncontaminated [0,1[uncontaminated to moderately contaminated [1,2[moderately contaminated [2,3[moderately to heavily contaminated [3,4[heavily contaminated [4,5[heavily to extremely contaminated ≥5 extremely contaminated
Pollution index (Alves et al., 2020)	$PI_i = \frac{C_i}{B_i}$	(10)	C_i is the concentration of element I; B_i is the geochemical background value of each element.	<1 low contamination [1,3[moderate [3,6[considerable [6,12[very high ≥12 extremely high
Contamination degree (Saha et al., 2024)	$CD = \sum_{i=1}^{n} PI_i$	(11)	Cumulative sum of the pollution indices for each element.	<6 low [6,12[moderate [12,24[significant ≥24 high
Integrated pollution load index (Alves et al., 2020)	$PLI = (PI_1 \times PI_2 \times PI_3 \times \cdots \times PI_n)^{1/n}$	(12)	PI is the pollution index of each element; n represents the number of elements determined.	0 background concentration]0,1] unpolluted]0,2] unpolluted to moderately polluted]2,3] moderately polluted]3,4] moderately to highly polluted]4,5] highly polluted >5 very highly polluted
Ecological risk factor (Alves et al., 2020)	$E_{r_i} = T_i \times PI_i$	(13)	T_i is the toxic-response factor for metal i (Cd, 30; As, 10; Sb, 7; Cu, 5; Ni, 5; Pb, 5; Co, 5; Cr, 2; V, 2; Zn, 1; Mn, 1; Ba, 1); PI is the pollution index of each element.	<40 low [40,80[moderate [80,160[considerable [160,320[high ≥320 very high
Potential ecological risk index (Alves et al., 2020)	$RI = \Sigma E_{ri}$	(14)	Sum of ecological risk factors of individual metal(loid)s	<150 low [150,300[moderate [300,600[considerable ≥600 high

(*continued on next page*)

Table 1 (*continued*)

Indices	Equations	Eq. number	Explanations	Contamination or risk degree
Nemerow pollution index (Saha et al., 2024)	$NPI = \sqrt{\frac{(PI_{mean})^2 + (PI_{max})^2}{2}}$	(15)	PI_{mean} and PI_{max} are the mean and maximum value of the PI_i of all metal(loid)s studied.	<0.7 unpolluted [0.7,1[warning line of pollution [1,2[little polluted [2,3[moderately polluted ≥3 highly polluted
Nemerow risk index (Varol et al., 2022)	$NRI = \sqrt{\frac{(Er_{mean})^2 + (Er_{max})^2}{2}}$	(16)	E_{rmean} and E_{rmax} are the mean and maximum value of E_{ri}.	≤40 low risk]40,80] moderate risk]80,160] considerable risk]160,320] high risk >320 very high risk
Toxic risk index (Varol et al., 2022)	$TRI = \frac{\sqrt{\frac{(C_i/TEL)^2 + (C_i/PEL)^2}{2}}}{\sum_{i=1}^{n}}$	(17)	C_i is the concentration of each element, TEL is the threshold effect level and PEL the permissible exposure level (Table S2 in the supplementary material).	≤5 no toxic risk]5,10] low toxic risk]10,15] moderate toxic risk]15,20] considerable toxic risk >20 very high toxic risk

by maximising between-group variance and minimising within-group variance.

2.4. Estimation of the contribution of mineral dust and sea salt to PM_{10}

To roughly estimate the contribution of mineral dust (MD) to the PM_{10} mass from constituents generally associated with crustal origin, elements were converted into their most common oxides. MD was calculated following the methodology described by Lokorai et al. (2021):

$$MD = [SiO_2] + [Al_2O_3] + [Fe_2O_3] + [CaO + CaCO_3] + [K_2O] + [MgO] + [TiO_2] \quad (1)$$

Calcium levels in its most abundant forms were estimated as follows:

$$[CaO + CaCO_3] = 1.95 \times [Ca] \quad (2)$$

Given that silicon was not analysed because the quartz filters are composed of this element, silica was estimated as:

$$SiO_2 = 3 \times [Al_2O_3] \quad (3)$$

The contribution of sea salt (SS) to PM_{10} levels was calculated using sodium (Na), a major sea salt component, along with typical elemental ratios for seawater and the Earth's crust (Querol et al., 2016). Non-sea salt Na (nssNa), sea salt Na (ssNa) and SS were estimated as:

$$nssNa = 0.348 \times Al \quad (4)$$

$$ssNa = Na - nssNa \quad (5)$$

$$SS = 3.26 \times ssNa \quad (6)$$

2.5. Contamination indices

To comprehensively assess the contamination levels and associated risks of PM_{10}-bound metal(loid)s, multiple contamination and risk indices were applied. Each index was selected based on its established use in environmental pollution studies and its ability to provide unique and complementary insights into contamination sources, severity, and potential ecological and health risks. Table 1 summarises the indices used, their equations, and their classification criteria.

The indices can be broadly categorised into three groups.

i) Source apportionment and anthropogenic influence
   - The Crustal Enrichment Factor (CEF) and Marine Enrichment Factor (MEF) distinguish between natural and anthropogenic contributions by normalising element concentrations against reference elements (e.g., Al, or Fe). EF values help identify whether elements primarily originate from crustal material, marine aerosols, or human activities such as industrial emissions and traffic-related sources.
   - The Geoaccumulation Index (I_{geo}) quantifies the degree of contamination relative to pre-industrial levels, allowing differentiation between unpolluted, moderately polluted, and heavily polluted environments.

ii) Overall contamination intensity
   - The Pollution Index (PI) and Contamination Degree (Cd) assess the extent of pollution for individual elements and the cumulative contamination from multiple pollutants, respectively.
   - The Integrated Pollution Load Index (PLI) provides an overall assessment of pollution severity by aggregating PI values across multiple elements, offering a single, comparable measure of contamination burden.

iii) Ecological and human health risk assessment

- The Ecological Risk Factor (ER) and Potential Ecological Risk Index (RI) evaluate the ecological impact of toxic elements, incorporating toxicity response coefficients to reflect the relative hazards of different pollutants.
- The Nemerow Pollution Index (NPI) and Nemerow Risk Index (NRI) account for the most contaminated element and the overall contamination level, emphasising extreme pollution scenarios that may require urgent intervention.
- The Toxic Risk Index (TRI) assesses potential human health risks by incorporating toxicological factors, providing insight into the likelihood of adverse health effects from exposure to specific elements.

By employing this suite of indices, a holistic assessment of PM_{10} contamination in Luanda is ensured, capturing both source-related information and potential environmental and health risks. The use of multiple indices prevents misinterpretation that could arise from relying on a single metric, as each index highlights different aspects of contamination.

2.6. Health risk assessment

Although exposure to pollutants can occur through inhalation, ingestion, or dermal contact, inhalation is the most significant pathway for airborne contaminants due to their direct entry into the respiratory system (SWA, 2013). To estimate health risks associated with inhalation exposure to PM_{10}-bound elements, average daily doses (ADDs) (expressed in μg/kg/day) were calculated for both children and adults using the methodology outlined by the USEPA (1986). These ADDs serve as the foundation for assessing both carcinogenic and non-carcinogenic health risks.

$$ADD_{inh} = \frac{C \times IR \times EF \times ED}{BW \times AT} \quad (18)$$

where,

C = Concentration of the pollutant in the air (μg/m^3)

IR = Inhalation rate (7.6 m^3/day for children or 20 m^3/day for adults)

EF = Exposure frequency (365 days/year)

ED = Exposure duration (6 years for children or 24 years for adults)

BW = Body weight (15 kg for children or 70 kg for adults)

AT = Averaging time (days); for non-carcinogenic effects, AT = ED × 365 days; for carcinogenic effects, AT = Lifetime (70 years × 365 days/year for adults; 18 years × 365 days/year for children)

The parameter values were taken from USEPA (2011).

To evaluate non-carcinogenic and carcinogenic effects, the hazard quotient (HQ), hazard index (HI), and carcinogenic risk (CR) were calculated (Alharbi et al., 2024). HQ represents the ratio of the average daily dose of an element to its reference dose for inhalation exposure (R_fD_{inh}). R_fD_{inh} (Table S3, supplementary material) represents the maximum daily exposure to an element that is unlikely to cause significant health effects over a lifetime. For some elements, reference doses are available only for oral exposure (R_fD_{oral}, μg/kg/day). In such cases, R_fD_{inh} was estimated as follows:

$$R_fD_{inh} = R_fD_{oral} \times \frac{BA_{oral}}{BA_{inh}} \quad (19)$$

where, BA_{oral} and BA_{inh} are the bioavailability fraction of each metal (loid) via oral and inhalation exposure, respectively (Table S3). HQ is the ratio of the potential exposure to an element and the level at which no adverse effects are expected. It is calculated as:

$$HQ = \frac{ADD_{inh}}{R_fD_{inh}} \quad (19a)$$

An HQ below 1 implies no anticipated adverse health effects, while an HQ above 1 indicates a potential risk of harm. HI is the combination of the individual HQs, offering an overall assessment of the potential for non-carcinogenic effects. An HI ≤ 1 suggests no significant risk of non-carcinogenic effects, while an HI > 1 indicates a potential risk, with the likelihood of such effects raising as the HI value increases. HI is estimated using the following equation:

$$HI = \sum HQ \quad (20)$$

CR represents the probability of an individual developing cancer over his lifetime as a result of exposure to carcinogenic hazards. According to USEPA, a CR below 1×10^{-6} is regarded as negligible, whereas a CR above 1×10^{-4} is likely to represent a significant risk to human health. CR is estimated as follows:

$$CR = \sum ADD \times SF \quad (21)$$

where SF is the slope factor, expressed in (μg/kg/day)$^{-1}$. This represents the increase in cancer risk per unit of daily exposure (in μg/kg/day) over a lifetime. A CR between 1×10^{-6} and 1×10^{-4} is considered an acceptable or tolerable risk for regulatory purposes, indicating that remediation is advisable.

3. Results and discussion

3.1. Concentrations and sources

PM_{10} concentrations ranged from 23.6 to 108 μg/m^3, averaging 59.3 μg/m^3. The 24-h guideline value of 45 μg/m^3 recommended by the World Health Organisation (WHO, 2021) was exceeded on 83% of days. According to the latest WHO ambient air quality database (WHO, 2024), in which annual concentrations for the 2010–2020 period are listed, much higher levels have been registered in South Asian cities, such as Chittagong, Bangladesh (102–155 μg/m^3), and in the Indian megacities of Delhi (192–292 μg/m^3) and Mumbai (49.7–136 μg/m^3). However, lower annual averages have been reported for the metropolis of São Paulo (27.3–36.6 μg/m^3), American cities such as Los Angeles (21.1–28.1 μg/m^3) and several European urban centres, including Paris, France (20.2–34.2 μg/m^3) and Coimbra, Portugal (16.8–26.2 μg/m^3).

During 35% of the measurement period, Luanda was influenced by "pure" Atlantic air masses (Fig. 1), which corresponded to the lowest PM_{10} concentrations (53.4 ± 9.8 μg/m^3). Air masses in cluster 4 followed a trajectory along the coastline from southern Angola, passing through areas with significant industrial activity, business centres, and dense population, resulting in the highest PM_{10} levels (68.7 ± 19.9 μg/m^3). Clusters 1 and 2 accounted for 27% and 22% of the measurement period, respectively, both originating from inland Angola but differing in their transport velocity.

MD contributed 31 ± 5.0% to the PM_{10} mass concentration during the entire sampling period, while SS represented 6.0 ± 5.0%. Dust has also been identified as a major contributor at multiple sampling points in the Vaal Triangle, a highly industrialised region of South Africa, accounting for 19–65% of the PM_{10} levels (Muyemeki et al., 2021). The contribution of soil dust to $PM_{2.5}$ in Addis Ababa, Ethiopia, was estimated at 17.4 ± 6.6% (Tefera et al., 2021). In Nairobi, Kenya, mineral dust was found to account for 35% of $PM_{2.5}$ (Gaita et al., 2014). As reported for other African cities, the high dust content in Luanda may be attributed, at least in part, to the extensive network of unpaved roads, particularly in the musseques, the city's informal settlements scattered all around the inner city where almost 2 million families live.

Soil-derived elements such as Ca, Al and Fe were among the most abundant analytes. In their oxide forms, they contributed, on average, 6.12%, 4.24%, and 2.49%, respectively, to the PM_{10} levels. Another abundant element in particulate matter was S (Table 2). In Angola, the S content in vehicle fuels is capped at 1500 ppm for both diesel and gasoline. This standard is part of the country's efforts to regulate air pollution, which includes transitioning to unleaded gasoline since 2005

and limiting the importation of older vehicles. However, Angola still faces challenges with enforcement mechanisms. This sulphur level is relatively high compared to global standards, especially in developed countries where S content in fuels is often limited to 10 ppm. The origin of S in PM_{10} can also be attributed to the refinery of Luanda. This industrial structure has undergone significant upgrades to improve its gasoline production capacity and reduce environmental impacts. A key part of these upgrades is the addition of a new platforming unit, which also includes initiatives for better energy efficiency by recycling gas. However, while the refinery is modernising, it has not adopted advanced desulphurisation technologies. The focus has been more on increasing gasoline production and reducing greenhouse gases through the use of hydrogen for power generation. Other prominent anthropogenic elements in PM_{10} were Zn, Ba, Pb and Cu. These are well known tracers of non-exhaust emissions resulting from tyre and brake wear (Adachi and Tainosho, 2004; Grigoratos and Martini, 2015; Thorpe and Harrison, 2008).

Elemental concentration ratios have been widely used to differentiate between predominant sources, particularly distinguishing geogenic from traffic non-exhaust emissions. To establish the elemental composition profile of brake wear emissions in Europe, Hulskotte et al. (2014) analysed 65 brake pads and 12 brake discs. The mean Fe/Cu ratio in brake pads was 2.0. In contrast, brake disc samples consisted almost entirely of iron (Fe), resulting in much higher Fe/Cu ratios. When assuming equal wear contributions from both pads and discs (50/50), the derived mean Fe/Cu ratio was 10.4. If a 70% disc and 30% pad wear contribution was hypothesised, the ratio increased to 22. This indicates that Fe/Cu ratios are influenced not only by brake formulations but also by the relative wear contributions of discs and pads, as well as by driving conditions. Casotti Rienda et al. (2023) reported average Fe/Cu ratios between 44.0 and 58.3 in PM_{10} from dust resuspension in parking lots. A mean Fe/Cu ratio of 40 was observed in the PM_{10} fraction of road dust samples collected in the city of Porto, Portugal (Alves et al., 2018). An average ratio of 22.2 was obtained in a stop-and-go traffic location in Grenoble, France, which was in close agreement with previous measurements in other kerbside locations in Europe (Charron et al., 2019). A much higher Fe/Cu ratio (121 ± 37.5) was observed in Luanda, suggesting that in addition to brake wear, there are likely other significant sources of iron. Two predominant geologic formations dominate the area in and around the city. The "Luanda" formation, covering most of the low-lying parts of the city and the coastline, consists of ferruginous sands, among other mineralogical materials. The ‘‘Quelo’’ or ‘‘red sands’’ formation dominates in the higher parts of the city, where iron-rich, sandy red soils have developed (Ferreira-Baptista and De Miguel, 2005). Thus, soil dust resuspension may be a significant source of iron for atmospheric aerosols in Luanda.

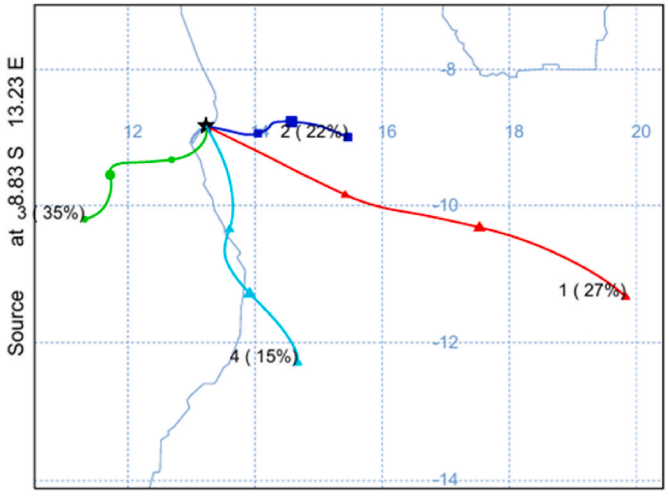

Fig. 1. HYSPLIT 5-day back trajectory cluster analysis for the measurement campaign and PM_{10} concentrations associated with each cluster.

The Cu/Sb ratios obtained in the present study (2.84 ± 0.91) clearly differ from the typical composition of the upper crust (Cu/Sb = 46.1; Wedepohl, 1995) and are close to the mean value of 2.2 found in ambient PM_{10} collected in a road tunnel in Braga, Portugal (Alves et al., 2015). Pant and Harrison (2013) reviewed the literature on ambient PM and compiled Cu/Sb ratios characteristic of brake wear particles, reporting values ranging from 1.3 to 9.1. Charron et al. (2019) compared Cu/Sb ratios from PM_{10} measurements in France (11.7 ± 5.1) with those described in the literature for London (9.1), Barcelona (7.0–7.9), Bern (13.2), Zurich (8.5), Sweden (4.6) and Vienna (1.6), stressing that some of the variability could be attributed to the adoption of Sb-free brake pads. It has also been suggested that the chemical composition of ambient PM does not fully replicate the original ingredients of the parent materials, as they are often altered by the high temperatures and pressures generated during the braking process (Grigoratos and Martini, 2015). Based on bibliographic data, Ramírez et al. (2019) argued that a Zn/Sb ratio of less than 25 is typical of brake wear particles, while higher values point to tyre wear. The researchers obtained an average ratio of 58 ± 28 in the PM_{10} fraction of road dust in the megacity of Bogota, Colombia, which falls between the values reported in previous studies for Barcelona (7.66–12.3) and New Delhi (68). In Luanda this ratio showed great variability (43 ± 40) but seems to confirm that Zn primarily originates from tyres. However, it should be noted that the industrial belt of Luanda, extending from the North to the East beyond the musseques, includes a zinc smelter. Depending on wind direction, this smelter may also contribute to the Zn levels in the city centre.

Although it may result from natural emissions, vanadium (V) is primarily utilised in the steel industry to produce high-strength, low-alloy steels (e.g., Crowther and Li, 2022). In the industrial belt of Luanda, especially in the neighbouring municipality of Viana, there is metallurgy industry, including steel production. Stainless steel is a Fe-based alloy containing Cr and other elements, including V (Badeshia and Honeycombe, 2017). Thus, emissions from this activity may eventually contribute to the composition of PM_{10} sampled in the city centre. A weak correlation between V and Cr (r^2 = 0.39) suggests that these elements do not strongly co-vary, indicating that they likely originate from different dominant sources. The strong correlation between V and Fe (r^2 = 0.80) and the moderate correlation between Cr and Fe (r^2 = 0.50) suggest that Cr and Fe may have partially overlapping sources but are not necessarily from the same origin. The strong V-Fe correlation implies that these two elements may share common sources (e.g., soil, heavy oil combustion), while the steel industry appears to be a less probable source of V. Vanadium is also employed as a heterogeneous catalyst, particularly in the treatment of vehicle exhaust emissions. Furthermore, V is found in both crude oil and coal, with concentrations varying greatly. In crude oil, V tends to accumulate in the heaviest distillation fractions and can reach elevated levels in by-products such as residual oil and petroleum coke. Thus, metallurgical industries, the oil refinery and emissions from traffic and ships may contribute to PM_{10}-bound vanadium in the atmosphere of Luanda. To identify possible sources of vanadium, a Ce-La-V ternary diagram was employed (Fig. 2). In constructing this graph, the concentrations of Ce and La were adjusted by multiplying them by appropriate factors (1.54 for Ce and 3.1 for La), allowing the centre of the diagram to represent the typical composition of the upper continental crust (Bozlaker et al., 2019; Conca et al., 2019; Turetta et al., 2021). Data points clustering near the diagram’s centre suggest that V in PM_{10} originates predominantly from upper crust weathering rather than anthropogenic sources such as oil combustion. Additionally, the V/Ni ratio was examined as an indicator of oil combustion sources, as both elements are enriched in crude oil and its combustion products. Moreno et al. (2010) reported that high V/Ni values (>4) can be used to trace the influence of nearby high-V pet coke and fuel oil combustion emissions. In Luanda, 71% of the V/Ni ratios were below or close to 1.75, which corresponds to the typical value for

Table 2
Concentrations of PM_{10}-bound elements in Luanda.

		Min.	Max.	Average	Std. Dev.	Median	No. of samples < detection limit (N = 129)
Minor (ng/m^3)	Li	0.159	1.43	0.500	0.211	0.454	
	Be	<0.00184	0.120	0.030	0.020	0.028	6
	Sc	0.0680	0.510	0.210	0.0818	0.197	
	V	0.854	5.32	2.24	0.806	2.09	
	Cr	0.529	9.33	3.48	1.32	3.52	
	Co	0.142	0.748	0.397	0.121	0.388	
	Ni	<0.397	13.4	4.51	3.90	3.63	3
	Cu	3.02	55.8	10.5	6.16	8.94	
	Zn	14.8	868	159	163	87.7	
	Ga	0.138	0.841	0.408	0.143	0.386	
	Ge	<0.0476	0.331	0.0163	0.0532	<0.0476	114
	As	0.290	0.988	0.531	0.167	0.488	
	Se	<0.0112	0.287	0.145	0.0518	0.137	1
	Rb	0.851	6.00	2.69	1.09	2.52	
	Sr	2.57	15.2	7.00	2.03	6.62	
	Y	<0.014	0.840	0.347	0.149	0.311	
	Zr	<0.0967	6.17	2.98	1.23	2.90	1
	Nb	0.120	0.634	0.354	0.106	0.342	
	Mo	<0.431	10.0	2.10	2.26	1.27	49
	Cd	0.111	3.33	0.563	0.533	0.401	
	Sn	0.420	5.28	1.74	0.840	1.49	
	Sb	1.23	14.1	3.74	1.55	3.43	
	Cs	0.0105	0.150	0.0637	0.0296	0.0630	
	Ba	8.19	101	43.2	20.4	36.2	
	La	0.270	1.60	0.776	0.261	0.735	
	Ce	0.571	3.35	1.66	0.567	1.59	
	Pr	0.0601	0.368	0.173	0.0608	0.163	
	Nd	0.220	1.33	0.613	0.219	0.584	
	Sm	0.00882	0.247	0.114	0.0422	0.109	
	Eu	0.00772	0.0570	0.0287	0.0102	0.0268	
	Gd	<0.00850	0.290	0.152	0.0540	0.152	7
	Tb	<0.00200	0.0391	0.0179	0.00765	0.0182	1
	Dy	<0.0087	0.195	0.0841	0.0382	0.0806	11
	Ho	<0.00120	0.0392	0.0183	0.00726	0.0172	1
	Er	<0.00340	0.105	0.0465	0.0196	0.0433	1
	Tm	<0.000340	0.0147	0.00693	0.00282	0.00643	1
	Yb	<0.00223	0.103	0.0438	0.0173	0.0410	1
	Lu	<0.000234	0.0142	0.00679	0.00279	0.00635	1
	Hf	0.00018	0.00537	0.00145	0.000904	0.00127	
	Ta	<0.000137	0.189	0.00279	0.0183	<0.000137	74
	W	0.0233	0.155	0.0681	0.0221	0.0666	
	Tl	0.0107	0.542	0.0526	0.0560	0.0402	
	Pb	1.82	126	17.8	22.2	8.00	
	Bi	0.0223	0.329	0.109	0.0637	0.0894	
	Th	<0.0084	0.567	0.250	0.102	0.229	1
	U	<0.0207	0.254	0.134	0.0480	0.142	2
Major (μg/m^3)	Al	0.398	3.01	1.35	0.544	1.28	
	Ca	0.832	4.20	2.56	0.677	2.46	
	Fe	0.326	2.54	1.14	0.358	1.10	
	K	0.0738	2.21	0.688	0.495	0.535	
	Mg	0.194	1.32	0.453	0.180	0.411	
	Mn	<0.00300	0.0687	0.0177	0.0144	0.0152	12
	Na	0.449	2.53	1.38	0.532	1.29	
	P	0.0177	0.132	0.0592	0.0250	0.0558	
	S	0.604	2.77	1.15	0.428	0.986	
	Ti	0.0267	0.191	0.0781	0.0281	0.0725	

the upper continental crust (Wedepohl, 1995). Only 12% of the samples showed V/Ni values greater than 4. Benetello et al. (2018) presented V/Ni ratios between 0.1 and 0.9 as typical of vehicle emissions. Thus, the V/Ni ratios in Luanda suggest a mix of soil contributions and vehicle emissions.

3.2. Contamination degree

The CEF values demonstrated that lanthanides, along with several other elements (e.g., K, Li, Be, Sc, Rb, Sr, Zr, etc.), were mostly geogenic (Fig. 3). In contrast, extremely high enrichments were obtained for Sb, Cd, Zn, Se, S, Pb, Bi, Cu, and Sn, reflecting their anthropogenic origin. Nearly all elements revealed non-marine sources, presenting MEF values well above 100. The only exceptions were Sr and Mg, which were not enriched relative to seawater. Negative geoaccumulation indices (I_{geo}) were observed for the lithophile elements Fe, Ca and Al, indicating no contamination. On the other hand, Cu, Sn, and Pb fell into the category of moderate to heavy contamination, Zn, Se, and Bi were classified as heavily contaminated, Cd as heavily to extremely contaminated, and Sb as extremely contaminated. The average pollution indices further confirmed considerable or very high contamination for many anthropogenic elements such as Sb (207), Cd (88.3), Se (30.2), Zn (50.3), S (20.2), Pb (16.4), Bi (14.8), Cu (12.5), Sn (11.6), As (4.5) and N (3.9), most of which are associated with traffic emissions. The cumulative sum of the individual pollution indices revealed an extremely high contamination degree (CD = 483 ± 174).

On average, low ecological risks were observed for V (1.42), Cr (3.38), Ni (19.5), Co (2.90), Ba (1.08), and Mn (0.59). In contrast,

moderate E_{ri} were obtained for Cu (62.5), Zn (50.3), and As (45.0), considerable for Pb (82.2), and very high for Cd (2649) and Sb (1446). Globally, a very high potential ecological risk index was found (RI = 4360 ± 2440). The ecological risk was mostly due to Cd and Sb, which accounted for 56 ± 13% and 38 ± 13% of RI, respectively. Non-steel brake pads used in automobile disc brake systems incorporate stibnite (Sb_2S_3) as a solid lubricant, helping to reduce friction material wear under high load conditions. During braking, Sb_2S_3 undergoes oxidation, resulting in the formation of Sb_2O_3, which is considered a potential human carcinogen (von Uexküll et al., 2005). Cadmium is utilised in the electroless nickel-cadmium bath phase during brake manufacturing, contributing to the brake coating that results in corrosion-resistant brake components (Talebzadeh et al., 2021). It is also used as a component in tyre tread rubbers, serves as a fundamental constituent in various types of batteries, is a by-product of zinc metal refining, and can be emitted in trace amounts from motor oil combustion and cement manufacturing. Cd is highly toxic to humans, causing severe damage to the kidneys, lungs, and bones with prolonged exposure (ATSDR, 2012).

Very high pollution load indices were observed for 7 elements (mean values): Sb (207), Cd (88.3), Zn (50.3), Se (30.2), Cu (12.5), Sn (11.6) and As (4.5). However, the integrated pollution load index, which is calculated as the geometric mean of the contamination for multiple elements, presented a mean close to 1, a value typical of baseline pollution levels. If the pollution indices of most elements are close to the baseline ($PI_i \approx 1$) or below it ($PI_i < 1$), they can offset the effect of a few elements with very high PI_i, pulling the overall PLI closer to 1. The PLI gives equal weight to all elements by using the geometric mean, regardless of whether certain elements are particularly significant contributors to pollution or pose greater risks. High PLI values for individual metal(loid)s indicate specific sources of pollution, which require targeted mitigation. A global PLI close to 1 might suggest that overall pollution is not critical, but it can mask the severity of certain elements if not analysed individually.

The daily integrated Nemerow pollution index was always higher than 58.7, averaging 151 ± 64.5 (Fig. 4). This suggests that Luanda faces persistent and severe atmospheric pollution throughout the year. The elements that contribute most to the high NPI values were Sb, Cd, Zn, Cu, Se, Bi and S. In addition to traffic and industrial emissions, particularly from metal processing, many of these elements can also be emitted during biomass burning and, to a lesser extent, from agricultural fertilisers. Despite exceeding the "strongly polluted" threshold (NPI >3), with NPI values generally above 20 and reaching a peak of 52.8, Riyadh, Saudi Arabia, exhibits a lower contamination degree compared to the Angolan capital (Alharbi et al., 2024). Integrated NPI values ranging from 2.65 to 24.5 (average 8.65) in the warm season and from 2.90 to 11.0 (average 6.04) in the cold season have been reported for road dust samples collected in Tehran, Iran (Ali-Taleshi et al., 2022). In road dust samples from Beijing, China, the NIP value exceeded 1 at all sites and 2 at most sites. Additionally, NPI values at 25% of the evaluated sites were greater than 8, indicating a high level of integrated pollution (Men et al., 2018).

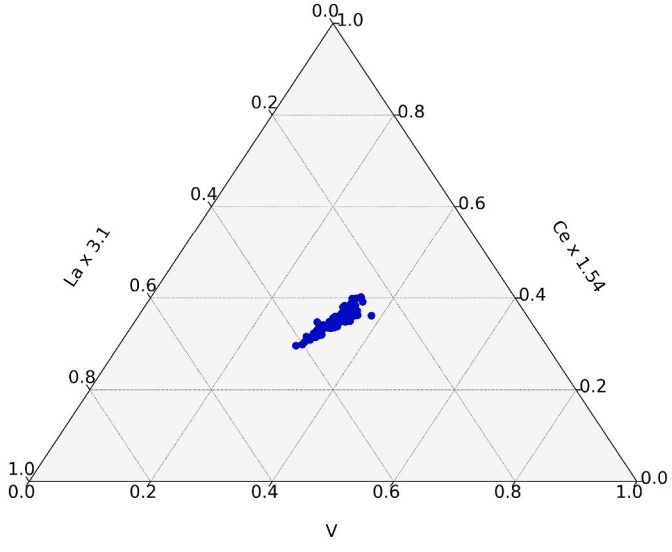

Fig. 2. Ce-La-V ternary diagram for PM_{10} samples collected in Luanda. The concentrations of Ce and La were adjusted (Ce × 1.54, La × 3.1) to align with the upper continental crust composition.

The Nemerow risk index (1990 ± 1530) confirmed an extremely high level of risk for the population of Luanda. The consistent pattern of high risk over the months highlights the urgent need for comprehensive air quality management strategies to mitigate these risks and protect public health. The NRI values reported by Alharbi et al. (2024) for daily PM_{10} samples collected in Riyadh frequently surpassed the threshold for very high risk (NRI >320). However, the minimum NRI value observed in Luanda (685) was higher than the peak documented for Riyadh (528), underscoring the severity of pollution in the Angolan capital. The very high risk in Luanda is once again demonstrated by the TRI values, which remained consistently above 23 (TRI = 124 ± 101). In Riyadh, the TRI values for PM_{10} generally fluctuated between low and very high toxic risk, but never surpassed 19.4 (Alharbi et al., 2024).

3.3. Assessment of potential health risks

A hazard index of 2.29 for children and 2.18 for adults was estimated, indicating non-cancer risks that exceed the acceptable threshold (Fig. 5). This suggests potential health concerns for both age groups. In addition to Si, the elements that contributed most significantly to HI were Fe, Mn, Be, Pb, Ni, Co, and Sb, each exhibiting HQ values exceeding 1. Si in the study area can originate from sources such as resuspended road dust, construction activities, or mineral dust. Amorphous and crystalline silica are common components of PM_{10}. Crystalline silica displays polymorphism in the form of quartz, tridymite, and crystoballite. Prolonged exposure to such polymorphic forms may contribute to the development of silicosis or even lead to lung cancer (Kamaludin et al., 2020; Nahin et al., 2022; Requena-Mullor et al., 2021). While silica-related health risks have been documented in industrial contexts, such as construction sites and the cement industry (Yeheyis et al., 2012; Kamaludin et al., 2020), studies specifically addressing the health risks of silica exposure in African urban environments are currently non-existent or extremely limited. This highlights the need for further research in Africa to better understand the implications of silica exposure in urban settings. Nonetheless, silica concentrations in urban PM_{10} have been shown to contribute to health risks globally, and the observed levels in Luanda warrant attention, particularly considering the potential for exposure to crystalline silica in the area.

Total carcinogenic risks from inhalation exposure to PM_{10}-bound elements were estimated at 2.34×10^{-3} for children and 1.36×10^{-3} for adults. Risks exceeding 1×10^{-4} (1 additional cancer case per 10,000 exposed individuals over a lifetime) are typically viewed as high and warrant intervention or mitigation. It should be noted that these risk estimates are conservative, as other hazardous PM_{10}-bound constituents, such as polycyclic aromatic hydrocarbons (PAHs), were not analysed in this study.

Although comparisons should be made with some caution, because the elements analysed may not coincide completely, other studies also have indicated worrying risks in several cities. Total non-carcinogenic risks of 1.07 and 3.11 were reported for adults and children, respectively, in an urban-industrial site in Acerra (Italy), a city located in an area called “triangle of death” (Di Vaio et al., 2018). In the same study, cumulative cancer risks of 1.4×10^{-5} for adults and 3.5×10^{-6} for children were obtained. HI values higher than 1 were documented for the Latin America’s largest opencast coal mine, located in northern

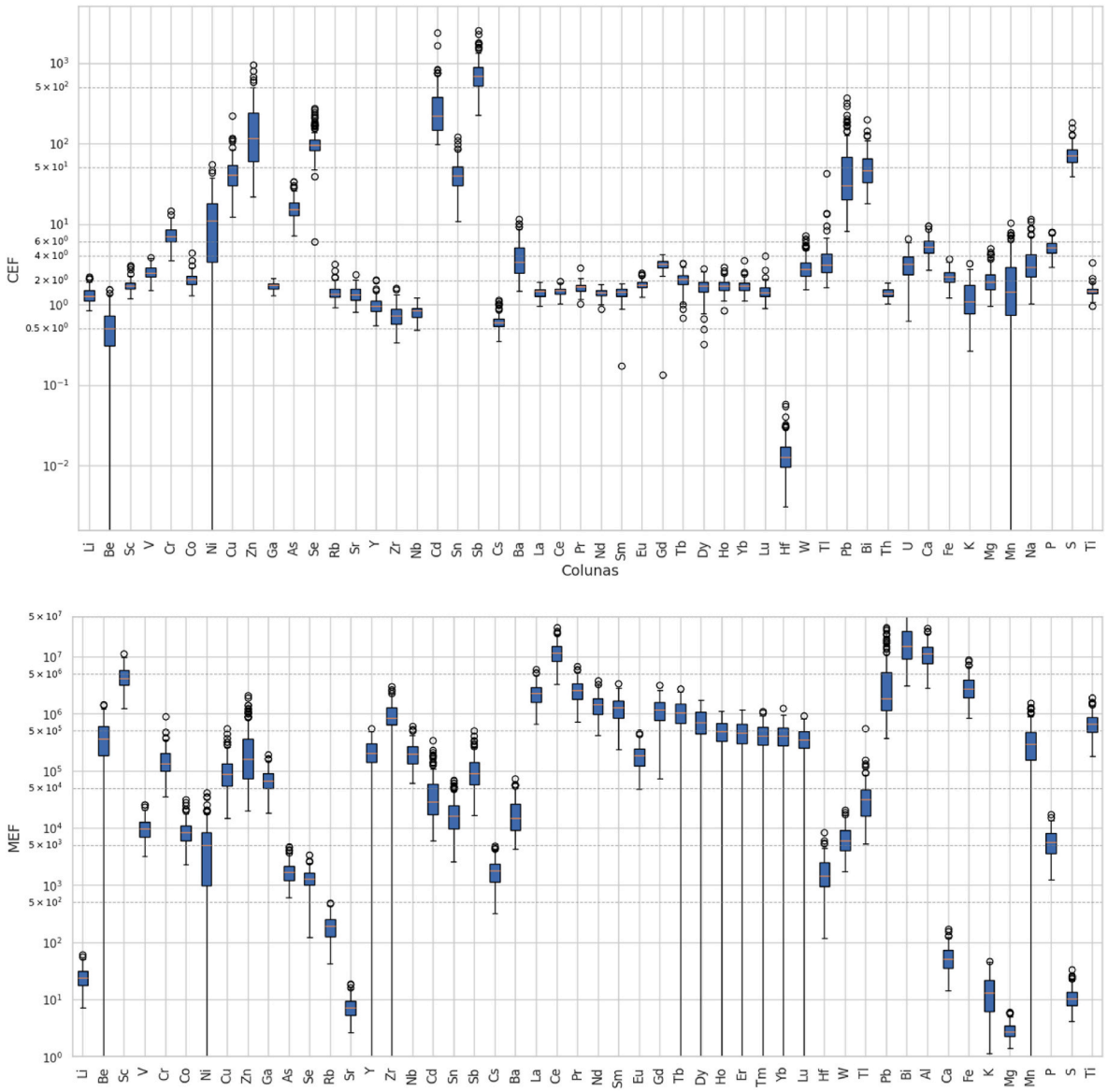

Fig. 3. Crustal and marine enrichment factors for PM_{10} collected in Luanda (The central line in each box represents the median (50th percentile); The box spans from the 1st quartile (Q1, 25th percentile) to the 3rd quartile (Q3, 75th percentile), representing the interquartile range (IQR); The whiskers extend to the smallest and largest values within 1.5 × IQR from Q1 and Q3, respectively; Outliers (individual points beyond the whiskers) are shown as dots and represent values outside the 1.5 × IQR range).

Colombia, with averages of 6.10, 3.32, and 3.61 for the north zone, south zone, and populated zone, respectively (Arregocés et al., 2023) . The corresponding mean CR values were 6.34×10^{-4}, 3.56×10^{-4} and 6.64×10^{-4}. Gosh et al. (2023) performed a comparative study of heavy metal pollution in ambient air and a health risk assessment in Durgapur as an industrial complex, Kolkata as an urban area, and Bolpur as a semi-urban region in West Bengal, India. The cumulative CR values were 4.08×10^{-5}, 2.35×10^{-5}, 1.01×10^{-5}, whereas the HI values were 4.66, 3.56 and 0.99, correspondingly. In the industrial towns of Ankleshwar and Vapi, in the region of Gujarat, India, hazardous indices of 158 and 138 were obtained for the adult population, respectively, while a value of 55.1 were estimated for both population groups (Nihalani et al., 2023). The cumulative cancer risks were 3.81×10^{-2} (Ankleshwar) and 3.73×10^{-2} (Vapi) for adults, and 1.49×10^{-2} (Ankleshwar) and 1.19×10^{-2} (Vapi) for children.

4. Conclusions

This study presents critical findings regarding the contamination levels and health risks associated with PM_{10} in Luanda, Angola. The data reveal that PM_{10} concentrations in the city consistently exceeded the WHO 24-h guideline of 45 μg/m^3, highlighting a significant public health concern. Although the observed PM_{10} levels in Luanda were lower than those recorded in major urban centres of South Asia, they surpassed the averages found in numerous cities across Europe, Brazil, and the United States.

Key sources of PM_{10}-bound elements in Luanda include: i) Mineral dust - Generated primarily from unpaved roads and local soils, mineral dust remains a persistent contributor to air pollution in the city; ii) Traffic emissions - Analysis of elemental ratios revealed substantial contributions from non-exhaust emissions associated with brake and tyre wear. Elements such as Cu and Zn served as indicators of this pollution source; iii) Industrial activities - Emissions from the petroleum refining sector and other industries were also identified as major

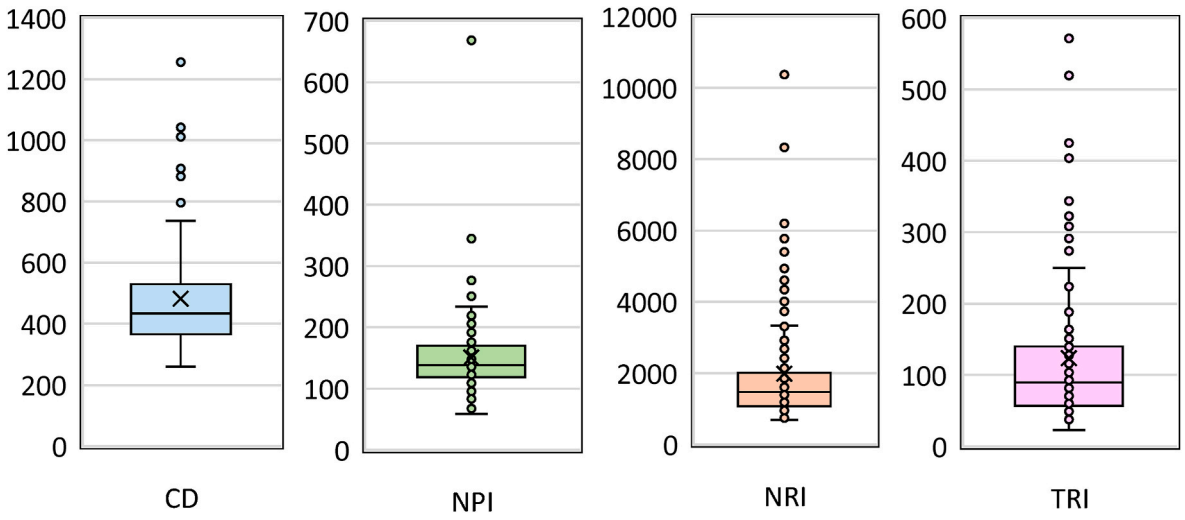

Fig. 4. Contamination degree, Nemerow pollution index, Nemerow risk index and toxic risk index of elements in PM_{10} from Luanda.

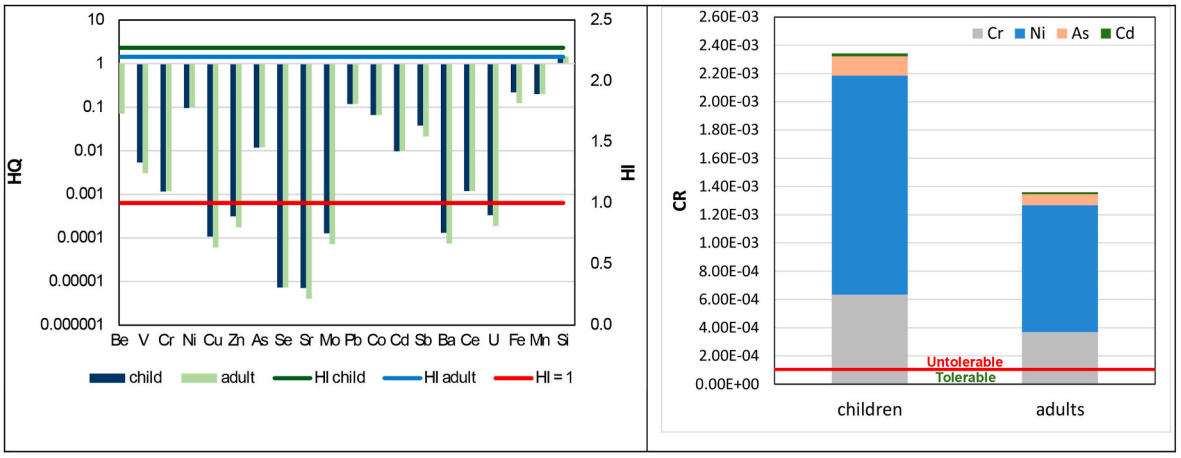

Fig. 5. Hazardous quotient, hazardous index and cancer risk associated with PM_{10}-bound elements in Luanda.

contributors to the PM_{10} burden, particularly the presence of toxic elements such as cadmium (Cd) and antimony (Sb), which pose significant ecological and health risks. The ecological risk assessment indicated extremely high values driven primarily by Cd and Sb, signaling the urgency for pollution control measures to mitigate long-term environmental degradation in Luanda. Moreover, the Nemerow risk index's critical values warn of persistent atmospheric pollution that could jeopardise public health.

Non-cancer and carcinogenic risks associated with PM_{10}-bound elements in Luanda exceed acceptable thresholds for both children and adults. The estimated carcinogenic risk suggests that a significant number of excess cancer cases could result from exposure to these pollutants. An estimated 234 excess cancer cases in children and 136 in adults per 100,000 individuals could occur over a lifetime of exposure. These findings draw our attention to the urgent need for intervention and mitigation strategies to reduce exposure to harmful air pollutants in Luanda. Immediate action is crucial to protect vulnerable populations, especially children, from the adverse effects of particulate matter. Furthermore, additional research is essential to refine risk estimates and better understand the long-term health impacts, particularly regarding silica, which remains under-researched in African urban contexts. The results also underline the importance of strengthening air quality management, including stricter regulations on traffic and industrial emissions. Future studies, particularly those employing Positive Matrix Factorisation (PMF) with extended datasets, will provide deeper insights into pollution sources and help guide effective policy. This study lays the groundwork for such research and stresses that, without timely intervention and comprehensive policy enforcement, Luanda is at risk of significant public health consequences due to escalating air pollution levels and associated risks.

CRediT authorship contribution statement

Célia A. Alves: Writing – original draft, Supervision, Resources, Project administration, Methodology, Investigation, Funding acquisition, Formal analysis, Conceptualization. **Ana Sanchez de la Campa:** Writing – review & editing, Methodology. **Yago Cipoli:** Writing – review & editing, Methodology, Formal analysis. **Leonardo Furst:** Methodology. **Gustavo Higawa:** Formal analysis. **Anabela Leitão:** Writing – review & editing, Resources. **Alan Victor da Silva:** Methodology. **Manuel S. Feliciano:** Writing – review & editing, Supervision.

Declaration of competing interest

The authors declare the following financial interests/personal relationships which may be considered as potential competing interests: Celia Alves, Yago Cipoli, and Leonardo Furst report financial support was provided by Foundation for Science and Technology. If there are other authors, they declare that they have no known competing financial interests or personal relationships that could have appeared to influence

the work reported in this paper.

Acknowledgements

The Portuguese Foundation for Science and Technology (FCT) is acknowledged for the PhD fellowships to L. Furst (SRFH/BD/08461/2020) and Y. Cipoli (SFRH/BD/04992/2021). The financial support to CESAM by FCT/MCTES (UIDP/50017/2020 + UIDB/50017/2020 + LA/P/0094/2020), through national funds, is also acknowledged. This work was developed within the project "Air Pollution in an African Megacity: Source Apportionment and Health Implications – APAM" (DOI: 10.54499/2022.04240.PTDC), financially supported by national funds (OE), through FCT/MCTES.

Appendix A. Supplementary data

Supplementary data to this article can be found online at https://doi.org/10.1016/j.envpol.2025.125995.

Data availability

Data will be made available on request.

References

Adachi, K., Tainosho, Y., 2004. Characterization of heavy metal particles embedded in tire dust. Atmos. Environ. 30, 1009–1017. https://doi.org/10.1016/j.envint.2004.04.004.

Adar, S.D., Filigrana, P.A., Clements, N., Peel, J.L., 2014. Ambient coarse particulate matter and human health: a systematic review and meta-analysis. Curr. Environ. Health Rep 1, 258–274. https://doi.org/10.1007/s40572-014-0022-z.

Alharbi, H.A., Rushdi, A.I., Bazeyad, A., Al-Mutlaq, K.F., 2024. Temporal variations, air quality, heavy metal concentrations, and environmental and health impacts of atmospheric $PM_{2.5}$ and PM_{10} in Riyadh City, Saudi Arabia. Atmosphere 15, 1448. https://doi.org/10.3390/atmos15121448.

Ali-Taleshi, M.S., Squizzato, S., Feiznia, S., Carabalí, G., 2022. From dust to the sources: the first quantitative assessment of the relative contributions of emissions sources to elements (toxic and non-toxic) in the urban roads of Tehran, Iran. Microchem. J. 181, 107817. https://doi.org/10.1016/j.microc.2022.107817.

Alves, C.A., Evtyugina, M., Vicente, A.M.P., Vicente, E.D., Nunes, T.V., Silva, P.M.A., Duarte, M.A.C., Pio, C.A., Amato, F., Querol, X., 2018. Chemical profiling of PM_{10} from urban road dust. Sci. Total Environ. 634, 41–51. https://doi.org/10.1016/j.scitotenv.2018.03.338.

Alves, C.A., Vicente, E.D., Casotti Rienda, I., Tomé, M., Querol, X., Amato, F., 2020. Loadings, chemical patterns and risks of inhalable road dust particles in an Atlantic city in the north of Portugal. Sci. Total Environ. 737, 139596. https://doi.org/10.1016/j.scitotenv.2020.139596.

Alves, C.A., Gomes, J., Nunes, T., Duarte, M., Calvo, A., Custódio, D., Pio, C., Karanasiou, A., Querol, X., 2015. Size-segregated particulate matter and gaseous emissions from motor vehicles in a road tunnel. Atmos. Res. 153, 134–144. https://doi.org/10.1016/j.atmosres.2014.08.002.

Amato, F., Alastuey, A., Karanasiou, A., Lucarelli, F., Nava, S., Calzolai, G., Severi, M., Becagli, S., Gianelle, V.L., Colombi, C., Alves, C., Custódio, D., Nunes, T., Cerqueira, M., Pio, C., Eleftheriadis, K., Diapouli, E., Reche, C., Minguillón, M.C., Manousakas, M., Maggos, T., Vratolis, S., Harrison, R.H., Querol, X., 2016. AIRUSE-LIFE+: a harmonized PM speciation and source apportionment in 5 Southern European cities. Atmos. Chem. Phys. 16, 3289–3309. https://doi.org/10.5194/acp-16-3289-2016.

Arregocés, H.A., Bonivento, G.J., Ladino, L.A., Beristain-Montiel, E., Restrepo, G., Miranda, J., Alvarez-Ospina, H., Rojano, R., 2023. Human health risk assessment of PM_{10}-bound heavy metals and PAHs around the Latin America's Largest opencast coal mine. Environ. Sci. Pollut. Res. 30, 125915–125930. https://doi.org/10.1007/s11356-023-30787-z.

ATSDR, 2012. Toxicological profile for cadmium. U.S. Department of health and human services. Public Health Service, Agency for Toxic Substances and Disease Registry. Available at: https://www.atsdr.cdc.gov/toxprofiles/tp5.pdf. Oct. 14th 2024.

Badeshia, H., Honeycombe, R., 2017. Chapter 12 - stainless steel. In: Steels: Microstructure and Properties, fourth ed. Elsevier, Oxford, UK, pp. 343–376. https://doi.org/10.1016/B978-0-08-100270-4.00012-3.

Benetello, F., Squizzato, S., Masiol, M., Khan, M.B., Visin, F., Formenton, G., Pavoni, B., 2018. A procedure to evaluate the factors determining the elemental composition of $PM_{2.5}$. Case study: the Veneto region (northeastern Italy). Environ. Sci. Pollut. Res. 25, 3823–3839. https://doi.org/10.1007/s11356-017-0759-7.

Boman, J., Shaltout, A.A., Abozied, A.M., Hassan, S.K., 2013. On the elemental composition of $PM_{2.5}$ in central Cairo, Egypt. X Ray Spectrom. 42, 276–283. https://doi.org/10.1002/xrs.2464276.

Bozlaker, A., Prospero, J.M., Price, J., Chellam, S., 2019. Identifying and quantifying the impacts of advected North African dust on the concentration and composition of airborne fine particulate matter in Houston and Galveston, Texas. J. Geophys. Res. Atmos. 124 (12). https://doi.org/10.1029/2019JD03079, 282–12,300.

Brunekreef, B., Forsberg, B., 2005. Epidemiological evidence of effects of coarse airborne particles on health. Eur. Respir. J. 26, 309–318. https://doi.org/10.1183/09031936.05.00001805.

Casotti Rienda, I., Alves, C.A., Nunes, T., Soares, M., Amato, F., Sánchez de la Campa, A., Kováts, N., Hubai, K., Teke, G., 2023. PM_{10} resuspension of road dust in different types of parking lots: emissions, chemical characterisation and ecotoxicity. Atmosphere 14, 305. https://doi.org/10.3390/atmos14020305.

Charron, A., Polo-Rehn, L., Besombes, J.L., Golly, B., Buisson, C., Chanut, H., Marchand, N., Guillaud, G., Jaffrezo, J.L., 2019. Identification and quantification of particulate tracers of exhaust and non-exhaust vehicle emissions. Atmos. Chem. Phys. 19, 5187–5207. https://doi.org/10.5194/acp-19-5187-2019.

Conca, E., Abollino, O., Giacomino, A., Buoso, S., Traversi, R., Becagli, S., Grotti, M., Malandrino, M., 2019. Source identification and temporal evolution of trace elements in PM_{10} collected near to Ny-Ålesund (Norwegian Arctic). Atmos. Environ. 203, 153–165. https://doi.org/10.1016/j.atmosenv.2019.02.001.

Crowther, D., Li, Y., 2022. The use of vanadium in high strength low alloy steels. 8th International Conference om High Strength Low Alloy Steels (HSLA 2022), 9-11 November 2022, Nanjing, China. https://vanitec.org/images/papers/051.pdf.

Di Vaio, P., Magli, E., Caliendo, G., Corvino, A., Fiorino, F., Frecentese, F., Saccone, I., Santagada, V., Severino, B., Onorati, G., Freda, G., Manzo, C., Perissutti, E., 2018. Heavy metals size distribution in PM_{10} and environmental-sanitary risk analysis in Acerra (Italy). Atmosphere 9, 58. https://doi.org/10.3390/atmos9020058.

Edlund, K.K., Killman, K., Molnár, P., Boman, J., Stockfelt, L., Wichmann, J., 2021. Health risk assessment of $PM_{2.5}$ and $PM_{2.5}$-bound trace elements in Thohoyandou, South Africa. Int. J. Environ. Res. Public Health 18, 1359. https://doi.org/10.3390/ijerph18031359.

Ferreira-Baptista, L., De Miguel, E., 2005. Geochemistry and risk assessment of street dust in Luanda, Angola: a tropical urban environment. Atmos. Environ. 39, 4501–4512. https://doi.org/10.1016/j.atmosenv.2005.03.026.

Gaita, S.M., Boman, J., Gatari, M.J., Pettersson, J.B.C., Janhäll, S., 2014. Source apportionment and seasonal variation of $PM_{2.5}$ in a Sub-Saharan African city: Nairobi, Kenya. Atmos. Chem. Phys. 14, 9977–9991. https://doi.org/10.5194/acp-14-9977-2014.

Ghosh, B., Padhy, P.K., Niyogi, S., Patra, P.K., Hecker, M., 2023. A comparative study of heavy metal pollution in ambient air and the health risks assessment in industrial, urban and semi-urban areas of West Bengal, India: an evaluation of carcinogenic, non-carcinogenic, and additional lifetime cancer cases. Environments 10, 190. https://doi.org/10.3390/environments10110190.

Grigoratos, T., Martini, G., 2015. Brake wear particle emissions: a review. Environ. Sci. Pollut. Res. 22, 2491–2504. https://doi.org/10.1007/s11356-014-3696-8.

Guo, J., Chai, G., Song, X., Hui, X., Li, Z., Feng, X., Yang, K., 2023. Long-term exposure to particulate matter on cardiovascular and respiratory diseases in low- and middle-income countries: a systematic review and meta-analysis. Front. Public Health 11, 1134341. https://doi.org/10.3389/fpubh.2023.1134341.

HEI, 2024. State of Global Air 2024. Special Report. Health Effects Institute, Boston, MA, USA. https://www.stateofglobalair.org/resources/report/state-global-air-report-2024.

Hopke, P.K., Dai, Q., Li, L., Feng, Y., 2020. Global review of recent source apportionments for airborne particulate matter. Sci. Total Environ. 740, 140091. https://doi.org/10.1016/j.scitotenv.2020.140091.

Hulskotte, J.H.J., Roskam, G.D., Denier van der Gon, H.A.C., 2014. Elemental composition of current automotive braking materials and derived air emission factors. Atmos. Environ. 99, 436–445. https://doi.org/10.1016/j.atmosenv.2014.10.007.

Jarvis, I.W.H., Enlo-scott, Z., Nagy, E., Mudway, I.S., Tetley, T.D., Arlt, V.M., Phillips, D. H., 2018. Genotoxicity of fine and coarse fraction ambient particulate matter in immortalised normal (TT1) and cancer-derived (A549) alveolar epithelial cells. Environ. Mol. Mutagen. 301, 290–301. https://doi.org/10.1002/em.22166.

Kamaludin, N.H., Jalaludin, J., Tamrin, S.B.M., Akim, A.M., Martiana, T., Widajati, N., 2020. Exposure to silica, arsenic, and chromium (VI) in cement workers: a probability health risk assessment. Aerosol Air Qual. Res. 20, 2347–2370. https://doi.org/10.4209/aaqr.2019.12.0656.

Kataoka, H., Tanaka, K., Tazuya-murayama, K., Yamashita, T., 2021. Cytotoxic effects of water-soluble extracts of coarse and fine atmospheric particulate matter on mast cell lines. Biol. Pharm. Bull. 44, 57–62. https://doi.org/10.1248/bpb.b20-00576.

Kolawole, T.O., Olatunji, A.S., 2023. Assessment of concentration of the potentially toxic elements and associated human health risk from particulate matter exposure along road intersections in Ibadan, southwestern Nigeria. Discov. Environ. 1, 3. https://doi.org/10.1007/s44274-023-00005-1.

Kumar, S., Saha, N., Mohana, A.A., Hasan, M.S., Rahman, M.S., Elmes, M.E., MacFarlane, G.R., 2024. Atmospheric particulate matter and associated trace elements pollution in Bangladesh: a comparative study with global megacities. Water Air Soil Pollut. 235, 222. https://doi.org/10.1007/s11270-024-07021-8.

Kyung, S.Y., Jeong, S.H., 2020. Particulate-matter related respiratory diseases. Tuberc. Respir. Dis. 83, 116–121. https://doi.org/10.4046/trd.2019.0025.

Lin, M., Yu, J.Z., 2020. Assessment of interactions between transition metals and atmospheric organics: ascorbic acid depletion and hydroxyl radical formation in organic-metal mixtures. Environ. Sci. Technol. 54, 1431–1442. https://doi.org/10.1021/acs.est.9b07478.

Lin, M., Yu, J.Z., 2019. Effect of metal-organic interactions on the oxidative potential of mixtures of atmospheric humic-like substances and copper/manganese as investigated by the dithiothreitol assay. Sci. Total Environ. 697, 134012. https://doi.org/10.1016/j.scitotenv.2019.134012.

Lokorai, K., Ali-Khodja, H., Khardi, S., Bencharif-Madani, F., Naidja, L., Bouziane, M., 2021. Influence of mineral dust on the concentration and composition of PM_{10} in the city of Constantine. Aeolian Res. 50, 100677. https://doi.org/10.1016/j.aeolia.2021.100677.

Men, C., Liu, R., Wang, Q., Guo, L., Shen, Z., 2018. The impact of seasonal varied human activity on characteristics and sources of heavy metals in metropolitan road dusts. Sci. Total Environ. 637–638, 844–854. https://doi.org/10.1016/j.scitotenv.2018.05.059.

Moreno, T., Querol, Q., Alastuey, A., de la Rosa, J., Sánchez de la Campa, A.M., Minguillón, M.C., Pandolfi, M., González-Castanedo, Y., Monfort, E., Gibbons, W., 2010. Variations in vanadium, nickel and lanthanoid element concentrations in urban air. Sci. Total Environ. 408, 4569–4579. https://doi.org/10.1016/j.scitotenv.2010.06.016.

Muyemeki, L., Burger, R., Piketh, S.J., Language, B., Beukes, J.P., Van Zyl, P.G., 2021. Source apportionment of ambient $PM_{10-2.5}$ and $PM_{2.5}$ for the Vaal Triangle, South Africa. S. Afr. J. Sci. 117. https://doi.org/10.17159/sajs.2021/8617. Art. #8617.

Nahin, M.N.I., Nahian, S., Islam, M.S., Roy, S., Jeba, F., Salam, A., 2022. Estimation and health risk assessment of respirable silica in the ambient particulate matter of Dhaka city. Dhaka Univ. J. Sci. 70, 35–41. https://doi.org/10.3329/dujs.v70i2.62604.

Nihalani, S., Jariwala, N., Khambete, A., 2023. Human health risk assessment of trace elements in PM_{10} for industrial areas in Gujarat. J. Air Pollut. Health 8, 117–134. https://doi.org/10.18502/japh.v8i2.12913.

Pant, P., Harrison, R.H., 2013. Estimation of the contribution of road traffic emissions to particulate matter concentrations from field measurements: a review. Atmos. Environ. 77, 78–97. https://doi.org/10.1016/j.atmosenv.2013.04.028.

Querol, et al., 2016. Contribution of natural sources to PM concentration levels. Report 7 of the AIRUSE LIFE 11 ENV/ES/584 Project. IDAEA-CSIC, Barcelona, Spain.

Querol, X., Alastuey, A., Rodriguez, S., Plana, F., Ruiz, C.R., Cots, N., Massagué, G., Puig, O., 2001. PM_{10} and $PM_{2.5}$ source apportionment in the Barcelona metropolitan area, Catalonia, Spain. Atmos. Environ. 35, 6407–6419. https://doi.org/10.1016/S1352-2310(01)00361-2.

Requena-Mullor, M., Alarcón-Rodríguez, R., Parrón-Carreño, T., Martínez-López, J.J., Lozano-Paniagua, D., Hernández, A.F., 2021. Association between crystalline silica dust exposure and silicosis development in artificial stone workers. Int. J. Environ. Res. Public Health 18, 5625. https://doi.org/10.3390/ijerph18115625.

Ramírez, O., Sánchez de la Campa, A.M., Amato, F., Moreno, T., Silva, L.F., de la Rosa, J. D., 2019. Physicochemical characterization and sources of the thoracic fraction of road dust in a Latin American megacity. Sci. Total Environ. 652, 434–446. https://doi.org/10.1016/j.scitotenv.2018.10.214.

Rodrigo-Moreno, A., Poschenrieder, C., Shabala, S., 2013. Transition metals: a double edge sward in ROS generation and signaling. Plant Signal. Behav. 8, e23425. https://doi.org/10.4161/psb.23425.

Rolph, G., Stein, A., Stunder, B., 2017. Real-time Environmental Applications and Display sYstem: READY. Environ. Model. Softw. 95, 210–228. https://doi.org/10.1016/j.envsoft.2017.06.025.

Sacks, J.D., Stanek, L.W., Luben, T.J., Johns, D.O., Buckley, B.J., Brown, J.S., Ross, M., 2011. Particulate matter–induced health effects: who is susceptible? Environ. Health Perspect. 119, 446–454. https://doi.org/10.1289/ehp.1002255.

Saha, A., Gupta, B.S., Patidar, S., Martínez-Villegas, N., 2024. Contamination risk assessment and distribution of rare trace metal(loid)s in surface soil of Cerrito Blanco, Mexico using various contamination indices. Total Environ. Adv. 9, 200086. https://doi.org/10.1016/j.teadva.2023.200086.

Santibáñez-Andrade, M., Quezada-Maldonado, E.M., Rivera-Pineda, A., Chirino, Y.I., García-Cuellar, C.M., Sánchez-Pérez, Y., 2023. The road to malignant cell transformation after particulate matter exposure: from oxidative stress to genotoxicity. Int. J. Mol. Sci. 24, 1782. https://doi.org/10.3390/ijms24021782.

Sarkar, S., Ribas-Santiago, C.E., Ibironke, O.A., Carranza, C., Meng, Q., Osorio-Vargas, A., Zhang, J., Torres, M., Chow, J.C., Watson, J.G., Ohman-Strickland, P., Schwander, S., 2019. Season and size of urban particulate matter differentially affect cytotoxicity and human immune responses to *Mycobacterium* tuberculosis. PLoS One 1–20. https://doi.org/10.1371/journal.pone.0219122.

Schins, R.P.F., Knaapen, A.D.M., Weishaupt, C., Winzer, A., Borm, P.J.A., 2002. Cytotoxic and inflammatory effects of coarse and fine particulate matter in macrophages and epithelial. Ann. Occup. Hyg. 46, 203–206. https://doi.org/10.1093/annhyg/46.suppl_1.203.

Shetaya, W.H., El-Mekawy, A., Hassan, S.K., 2024. Tempo-spatial variability and health risks of $PM_{2.5}$ and associated metal(loid)s in Greater Cairo, Egypt. Expo. Health 16, 973–988. https://doi.org/10.1007/s12403-023-00603-7.

Spagnolo, A.M., Ottria, G., Perdelli, F., Cristina, M.L., 2015. Chemical characterisation of the coarse and fine particulate matter in the environment of an underground railway system: cytotoxic effects and oxidative stress - a preliminary study. Int. J. Environ. Res. Public Health 12, 4031–4046. https://doi.org/10.3390/ijerph120404031.

Stein, A.F., Draxler, R.R., Rolph, G.D., Stunder, B.J.B., Cohen, M.D., Ngan, F., 2015. NOAA's HYSPLIT atmospheric transport and dispersion modeling system. B. Am. Meteorol. Soc. 96, 2059–2077. https://doi.org/10.1175/BAMS-D-14-00110.1.

Sulaymon, D., Mei, X., Yang, S., Chen, S., Zhang, Y., Hopke, P.K., Schauer, J.J., Zhang, Y., 2020. $PM_{2.5}$ in Abuja, Nigeria: chemical characterization, source apportionment, temporal variations, transport pathways and the health risks assessment. Atmos. Res. 237, 104833. https://doi.org/10.1016/j.atmosres.2019.104833.

SWA, 2013. Guidance on the interpretation of workplace exposure standards for airborne contaminants. Safe Work Australia. https://www.safeworkaustralia.gov.au/.

Talebzadeh, T., Valeo, C., Gupta, R., 2021. Cadmium water pollution associated with motor vehicle brake parts. IOP Conf. Ser. Earth Environ. Sci. 691, 012001. https://doi.org/10.1016/10.1088/1755-1315/691/1/012001.

Tang, Z., Cao, Z., Guo, X., Chen, H., Lian, Y., Zheng, W., Chen, Y., Lian, H., Hu, X., 2020. Cytotoxicity and toxicoproteomic analyses of human lung epithelial cells exposed to extracts of atmospheric particulate matters on PTFE filters using acetone and water. Ecotoxicol. Environ. Saf. 191, 110223. https://doi.org/10.1016/j.ecoenv.2020.110223.

Tchounwou, P.B., Yedjou, C.G., Patlolla, A.K., Sutton, D.J., 2012. Heavy metal toxicity and the environment. Exp. Suppl. 101, 133–164. https://doi.org/10.1007/978-3-7643-8340-4_6.

Tefera, W., Kumie, A., Berhane, K., Gilliland, F., Lai, A., Sricharoenvech, P., Patz, J., Samet, J., Schauer, J.J., 2021. Source Apportionment of fine organic particulate matter ($PM_{2.5}$) in Central Addis Ababa, Ethiopia. Int. J. Environ. Res. Public Health 18. https://doi.org/10.3390/ijerph182111608.

Tefera, W., Kumie, A., Berhane, K., Gilliland, F., Lai, A., Sricharoenvech, P., Samet, J., Patz, J., Schauer, J.J., 2020. Chemical characterization and seasonality of ambient particles ($PM_{2.5}$) in the city centre of Addis Ababa. Int. J. Environ. Res. Public Health 17, 6998. https://doi.org/10.3390/ijerph17196998.

Thorpe, A., Harrison, R.M., 2008. Sources and properties of non-exhaust particulate matter from road traffic: a review. Sci. Total Environ. 400, 270–282. https://doi.org/10.1016/j.scitotenv.2008.06.007.

Turetta, C., Feltracco, M., Barbaro, E., Spolaor, A., Barbante, C., Gambaro, A., 2021. A year-round measurement of water-soluble trace and rare Earth elements in Arctic aerosol: possible inorganic tracers of specific events. Atmosphere 12, 694. https://doi.org/10.3390/atmos12060694.

USEPA, 1986. Guidelines for the Health Risk Assessment of Chemical Mixtures. EPA/630/R-00/002. Office of Research and Development. United States Environmental Protection Agency, Washington DC.

USEPA, 2011. Exposure Factors Handbook, 2011 Edition. National Center for Environmental Assessment, Office of Research and Development, United States Environmental Protection Agency, Washington DC. EPA/600/R-09/052F.

Varol, M., Ustaoğlu, F., Tokatlı, C., 2022. Ecological risk assessment of metals in sediments from three stagnant water bodies in Northern Turkey. Curr. Pollut. Rep. 8, 409–421. https://doi.org/10.1007/s40726-022-00239-2.

von Uexküll, O., Skerfving, S., Doyle, R., Braungart, M., 2005. Antimony in brake pads – a carcinogenic component? J. Clean. Prod. 13, 19–31. https://doi.org/10.1016/J.JCLEPRO.2003.10.008.

Wedepohl, H.K., 1995. The composition of the continental crust. Geochim. Cosmochim. Acta 59, 1217–1232. https://doi.org/10.1016/0016-7037(95)00038-2.

WHO, 2021. In: WHO global air quality guidelines: particulate matter ($PM_{2.5}$ and PM_{10}), ozone, nitrogen dioxide, sulfur dioxide and carbon monoxide. European Centre for Environment and Health, World Health Organization, Bonn, Germany. https://iris.who.int/handle/10665/345329.

WHO, 2024. WHO ambient air quality database (update Jan 2024). In: Environment, Climate Change and Health (ECH) Department, Air Quality, Energy and Health (AQE) Unit (V6.1), sixth ed. World Health Organization, Geneva, Switzerland. Available at: https://www.who.int/publications/m/item/who-ambient-air-quality-database-(update-jan-2024. October 7th, 2024.

Yeheyis, M., Aguilar, G., Hewage, K., Sadiq, R., 2012. Exposure to crystalline silica (Si) inhalation among construction workers: a probabilistic risk analysis. Hum. Ecol. Risk Assess. 18, 1036–1050. https://doi.org/10.1080/10807039.2012.707931.